Modeling Capillary Condensation in Cylindrical Nanopores: A Molecular Dynamics Study

Minoru Miyahara,* Hideki Kanda, Tomohisa Yoshioka,† and Morio Okazaki‡

Department of Chemical Engineering, Kyoto University, Kyoto 606-8501, Japan

Received September 16, 1999. In Final Form: January 27, 2000

We modeled condensation phenomena within cylindrical nanopores as a possible replacement for the Kelvin model that underestimates nanometer order pore sizes. The proposed model follows the simple concept of a continuum assumption similar to that for the Kelvin model. The difference was in the introduction of the contribution of the pore-wall potential and the curvature-dependent surface tension in our model. A molecular dynamics (MD) technique developed by the authors for isotherm determination was employed to test the concept and the model. Several isotherms for N_2-like Lennard-Jones (LJ) particles in a silicate-like cylindrical pore with various diameters from 2 to 4 nm were obtained through MD simulations, and a relation between pore diameter and critical condensation pressure was determined. The present model successfully described the relation to demonstrate its reliability. The validity of the proposed model was examined also from the aspect of the shape of the meniscus and the pressure profile in the condensed phase, and gave fairly good agreement.

1. Introduction

One of the most important applications of physical adsorption would be the pore size estimation. The Kelvin condensation model is widely used for the characterization especially for mesoporous solids, while many articles have reported its underestimation of pore size in the nanometer region.[1−3] The survival of the Kelvin model despite the underestimation is a direct reflection of the lack of an appropriate model that is accurate enough for nanopores as well as handy enough for widespread use. A straightforward application of statistical thermodynamics,[4−6] such as the density functional theory and molecular simulation technique could be a solution at the expense of simplicity. The aim here is to give a simple concept and a model to describe the condensation phenomena in nanopores.

We have studied the condensation in nanopores with the above situation in mind. We had proposed a new condensation model in slit-shaped nanopores,[7] and now are extending it to cylindrical pores. The concept is that the meniscus of the condensed phase need not have curvature to the extent expected by the Kelvin model because the attractive potential from pore walls also stabilizes the condensed phase. Thus the meniscus would exhibit nonuniform curvature. Surface tension deviated from that of a flat interface[8,9] is also taken into account.

A molecular dynamics (MD) technique developed by the authors[2] for isotherm determination is employed to test the concept and the model. The necessity of the molecular simulations or computer experiments instead of real experiments with existing materials came from the lack of an ideal porous material with perfectly known surface characteristics and with perfect uniformity in pore size: Either of the unknowns could be adjusted to obtain an apparent "good result" for the other, which could not stand for a direct verification of the condensation model. Employing a molecular simulation as an experimental system, a great advantage also arises: One can obtain detailed information of the condensed phase such as density distribution and the shape of the gas−condensate interface. The model can be tested not only for the critical condensation pressure but also for the above factors. In short, the model successfully described the relation to prove its validity. Thus verified in an ideal system, the model underwent another test in a real system with a mesoporous silicate FSM-16, which possesses a quite uniform pore size, and the results will be presented in the near future.

2. Condensation Model

2.1. Basic Concept. The curvature of the condensed phase is the primary reason that vapor condenses at a lower than saturated equilibrium pressure. The Kelvin equation describes the effect of a curved surface for condensation in the following form for cylindrical pores with zero contact angle:

$$kT \ln(p_g/p_{sat}) = -\frac{2\gamma V_p}{R - t} \quad (1)$$

where k is Boltzmann's constant, p is pressure, and the subscript g indicates gas phase and sat indicates saturation. γ is the surface tension of the liquid, V_p the volume per molecule of liquid, R the pore radius, and t is the thickness of adsorption film on a pore wall. The work needed to hold a material in the liquid state apart from the bulk vapor phase with lower pressure than p_{sat} is compensated solely by the pressure reduction within the condensed phase given by the Young−Laplace effect. In a nanoscale pore, however, the condensation phenomena must be influenced by other effects such as the external

* To whom correspondence should be addressed.
† Present address: Department of Chemical Engineering, Hiroshima University, Higashi-Hiroshima 793-0046, Japan.
‡ Present address: Polytech College Kyoto, Maizuru City, Kyoto Prefecture 624-0912, Japan.

(1) Evans, R.; Marconi, U. M. B.; Tarazona, P. *J. Chem. Phys.* **1986**, *84*, 2376.
(2) Miyahara, M.; Yoshioka, T.; Okazaki, M. *J. Chem. Phys.* **1997**, *106*, 8124.
(3) Saito, A.; Foley, H. C. *AIChE J.* **1991**, *37*, 429.
(4) Nicholson, D. *J. Phys. D* **1968**, *1*, 3416.
(5) Evans, R.; Marconi, U. M. B. *Chem. Phys. Lett.* **1985**, *114*, 415.
(6) Seaton, N. A.; Walton, J. P. R. B.; Quirke, N. *Carbon* **1989**, *27*, 853.
(7) Yoshioka, T.; Miyahara, M.; Okazaki, M. *J. Chem. Eng. Jpn.* **1997**, *30*, 274.
(8) Tolman, R. C. *J. Chem. Phys.* **1949**, *17*, 333.
(9) Melrose, J. C. *Ind. and Eng. Chem.* **1968**, *60*, 53.

10.1021/la991227e CCC: $19.00
Published on Web 03/22/2000

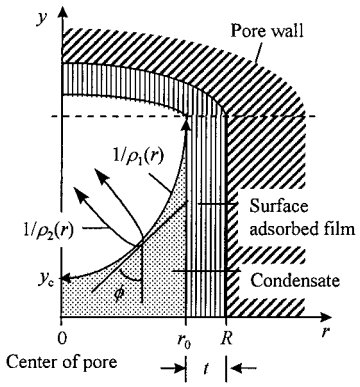

Figure 1. Schematic of gas−condensate interface and surface adsorption phase.

force field from the pore wall, the dependency of the surface tension on curvature, and the structural difference between normal liquid and adsorption phase confined within a narrow space.

We propose a new condensation model in which the external force field from the pore wall and the dependency of the surface tension on curvature are considered. In order to maintain simplicity, the model treats the fluid in a pore as a continuum throughout. Also for simplicity, the derivation is based on an idealized interface of tension, similar to the case for the Kelvin model. Including the above-mentioned two factors, the basic equation to describe the condensation is given as follows, referring to Figure 1:

$$kT \ln\left(\frac{p_g}{p_{sat}}\right) = \Delta\psi(r) - V_p\left(\frac{\gamma(\rho)}{\rho(r)}\right) \tag{2}$$

where

$$\frac{1}{\rho(r)} = \frac{1}{\rho_1(r)} + \frac{1}{\rho_2(r)}$$

$\rho_1(r)$ and $\rho_2(r)$ are the local radius of curvature of interface at a radial position r, and $\Delta\psi(r)$ is the contribution of the attractive potential energy from pore wall, which must be expressed as an "excess" amount compared with a potential energy that a molecule would feel if the pore wall is liquid consisting of the same molecules as adsorbate. The surface tension is treated as a function of the curvature because the radius of the curved interface in the nanopore is comparable with the thickness of the gas−liquid boundary layer and gives a considerable difference in surface tension from compared to a flat interface. The relation given by the Gibbs−Tolman−Koenig−Buff equation[9] is adopted for the curvature dependence, the details of which are given in Appendix A. The reason we have two different principal radii of curvature in eq 2, instead of the single radius of $(R-t)$ in the Kelvin model, comes from the existence of the potential energy term, which is location-dependent. Since the right-hand side of eq 2 must be constant regardless of the location, the contribution of the surface tension term varies with radial location and the two principal curvatures cannot be the same. In other words the meniscus is *not* hemispherical in the present model.

In principle, eq 2 determines the local curvature term for a given relative pressure. Since a geometric relation holds for the two principal curvatures, each of them can be known. Thus a geometric integration with respect to the shape of the interface can be made, which will give the pore size if summed with the thickness of the adsorbed film on the interior surface of the pore. Thus the relation of critical pore size and equilibrium vapor pressure can be obtained. This procedure is expressed quantitatively below.

2.2. Critical Condensation Pressure. Taking the origin of r at the center of the pore as in Figure 1, the first curvature of the interface along a vertical sectional plane is expressed as eq 3, with which the second curvature that is orthogonal to the first has a relation expressed by eq 4:

$$\rho_1(r) = \frac{dr}{d\cos\phi} \tag{3}$$

$$\rho_2(r) = \frac{r}{\cos\phi} = \frac{r}{\int_0^r \rho_1^{-1}(r)dr} \tag{4}$$

Rearranging eq 2 to give $\rho_1(r)$, and substituting eq 3, we have

$$\frac{d\cos\phi}{dr} = \frac{1}{\gamma(\rho)}\left[\frac{1}{V_p}\left\{\Delta\psi(r) - kT\ln\left(\frac{p_g}{p_{sat}}\right)\right\} - \frac{\gamma(\rho)}{\rho_2(r)}\right] \tag{5}$$

This equation, together with eq 4, will give the shape of the meniscus. Boundary conditions for forming the gas−liquid interface with the contact angle being zero are given by:

$$\text{B. C. 1: at } r = r_0,\ \phi = 0$$

$$\text{B. C. 2: at } r = 0,\ \phi = \pi/2$$

Integrating eq 5 formally, and applying the above boundary conditions, we obtain the constraint to be satisfied at critical condensation condition as follows.

$$1 = \int_0^{r_0} dr\, \frac{1}{\gamma(\rho)}\left[\frac{1}{V_p}\left\{\Delta\psi(r) - kT\ln\left(\frac{p_g}{p_{sat}}\right)\right\} - \frac{\gamma(\rho)}{\rho_2(r)}\right] \tag{6}$$

The position of the surface adsorbed film on the wall, r_0, is assumed to be given by the following equation since $1/\rho_1$ and $1/\rho_2$ are 0 and $1/r_0$, respectively.

$$kT\ln\left(\frac{p_g}{p_{sat}}\right) = \Delta\psi(r_0) - V_p\frac{\gamma(r_0)}{r_0} \tag{7}$$

The above expression of surface adsorption film is an analogue of the Frenkel theory for a planar surface with the additional second term, which comes from the surface tension of the interior cylindrical surface of the adsorbed film with radius r_0. The necessity of this term was examined with grand canonical Monte Carlo simulations, which compared the cases of adsorption on planar and cylindrical surfaces with the same potential energy. The details are explained in Appendix B.

Summarizing, eqs 4, 6, and 7, together with the Gibbs−Tolman−Koenig−Buff equation, should be solved simultaneously to find R, $t(= R - r_0)$, $\rho_1(r)$, and $\rho_2(r)$ for a given relative pressure. This numerical calculation, though it needs an iterative procedure, can be done quite easily, e.g., on a personal computer or even on a pocket computer.

2.3. Shape of the Interface. The Kelvin model implies that the curvature of the interface is constant yielding a hemispherical gas−condensate interface. On the other hand, the curvature is a function of r as shown in eqs 3 and 4 in the proposed model. Referring again to Figure 1, the relation of $dr/dy(r) = \tan\phi$ should hold along the meniscus. Denoting $y_c = y(0)$ at the center of the pore,

integration of the above geometric relation gives the shape of the interface as eq 8.

$$y(r) - y_c = \int_0^r \frac{dr}{\tan\phi} \tag{8}$$

The relation between ϕ and r can be resolved when obtaining the pore size, and the numerical integration of eq 8 can be executed to obtain the shape of the meniscus. Though the shape itself is not necessary for the pore size determination, this information will be used for testing the proposed model.

2.4. Pressure Profile. The Kelvin model assumes uniform curvature to have hemispherical interface, and hence only a constant pressure prevails within the condensed phase. On the other hand the proposed model implies a nonuniform pressure profile as a result of the nonhemispherical interface. Since the surface tension term in eq 2 comes from the pressure difference across the interface, the pressure profile within the condensed phase can be expressed as follows.

$$p_g - p_{ads}(r) = \frac{\gamma(\rho)}{\rho(r)} = \frac{\Delta\psi(r) - kT\ln(p_g/p_{sat})}{V_p} \tag{9}$$

We understand that, in nanopores, the pressure exhibits an anisotropic nature and a "pressure" cannot be treated the same as in the bulk phase. A more strict interpretation treating pressure as tensors, however, would bring much complexity into the model, which would defeat our purpose. Therefore the pressure within the condensed phase is expressed as an isotropic property at a given location r in a pore and the direction-dependence is not taken into account in this model. Again, though the pressure profile itself is not necessary for the pore size determination, this information will be used for another test of the present model.

3. MD Simulation

3.1. Simulation Scheme. The concept of the molecular dynamics (MD) technique developed by the authors[2] for isotherm determination in the slit pore is applied here with a slight modification for cylindrical pores. A possible alternative molecular simulation would include a grand canonical Monte Carlo (GCMC), as has often been employed for determination of adsorption equilibria. For capillary condensation, however, this method suffers from the difficulty in determining the true equilibrium between two metastable branches near the critical condensation pressure. One should calculate a grand potential to determine the true thermodynamic equilibrium, which needs many simulations including far higher temperature to obtain an isotherm without first-order transition, and then a thermodynamic integral. Other than the GCMC, one may employ a usual MD simulation followed by Widom's particle insertion method to determine the chemical potential of an adsorption system, but the procedure must be very complicated for this kind of highly heterogeneous system. High density also brings a difficulty in obtaining a sufficient number of successful insertions to obtain reliable statistical averages.

The unique feature of the present simulation cell is an imaginary gas phase with which the adsorbed phase can interact. Because of this interaction the equilibrium vapor pressure for a given number of molecules in pore space can be determined. Also, the simulation cell allows a stable interface to hold. Maybe because of the presence of the interface in the cell, the simulation scheme was free from hysteresis, and the relation between pore size and the critical vapor pressure for condensation was able to be obtained. Since the details of the simulation method are given elsewhere,[2] a brief description is made below.

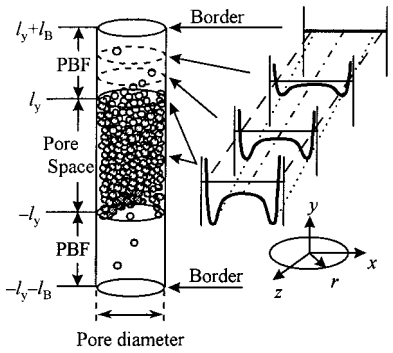

Figure 2. Schematic of unit cell and conceptual potential profile within the pore and potential buffering field.

Figure 2 shows the unit cell employed in this study. The central portion of the cell between $-l_y$ and $+l_y$ is the pore space with a full potential energy. At a location distant l_B from the edge of the full potential field, we set a border plane with an imaginary gas phase with which molecules in the pore can interact. Since the absolute value of external potential energy in the gas phase must be zero, there should exist a connecting space with the slope of potential energy between the gas phase and the pore space. This space is called potential buffering field (PBF). Molecules trying to desorb from the pore space must climb up the potential slope in PBF, and only those with sufficient kinetic energy can reach the border plane. If we set a perfect reflection condition at the border, the frequency of particles coming up should be a direct measure of the vapor pressure that is in equilibrium with the given adsorbed/condensed phase. Thus counting the molecules reaching the border, the equilibrium pressure can be determined.

The pore length was at least 8 nm so that the condensation phase had sufficient thickness and was free from any influence of the gas−liquid interface in the main body of the condensation phase. The length of PBF was 4 nm, with which a molecule reaching the border plane was free from interaction force from adsorbed phase.

3.2. Simulation Details. As a system for testing the proposed model, a LJ fluid in a structureless cylindrical pore made of LJ solid was employed. The adsorbate was nitrogen-like LJ fluid, having an interaction potential of

$$\phi_{gg}(r_{ij}) = 4\epsilon_{gg}\left[\left(\frac{\sigma_{gg}}{r_{ij}}\right)^{12} - \left(\frac{\sigma_{gg}}{r_{ij}}\right)^{6}\right] \tag{10}$$

with ϵ_{gg}/k and σ_{gg} being 95 K and 0.37 nm, respectively. The cutoff distance was $3.5\sigma_{gg}$. For a cylindrical pore wall, the potential function derived by Peterson et al.[10] with cylindrical coordinate integration, which is analogous to the LJ(9-3) potential for a planar solid surface, was used. The interaction and force between one adsorbate particle at a location r and the wall is given by

(10) Peterson, B. K.; Walton, J. P. R. B.; Gubbins, K. E. *J. Chem. Soc., Faraday Trans. 2* **1986**, *82*, 1789.

$$\phi_{gs}(r, R) = \pi\epsilon_{gs}\rho_s\left[\frac{7\sigma_{gs}^{12}}{32}K_9(r, R) - \sigma_{gs}^{6}K_3(r, R)\right] \quad (11)$$

$$F_{gs}(r, R) = \frac{d\phi_{gs}(r, R)}{dr} = \pi\epsilon_{gs}\rho_s\left[\frac{63\sigma_{gs}^{12}}{32}J_{10}(r, R) - 3\sigma_{gs}^{6}J_4(r, R)\right] \quad (12)$$

where

$$K_n(r, R) = R^{-n}\int_0^{\pi} d\Theta\left[-\frac{r}{R}\cos\Theta + \left(1 - \left(\frac{r}{R}\right)^2 \sin^2\Theta\right)^{1/2}\right]^{-n}$$

$$J_n(r, R) = R^{-n}\int_0^{\pi} d\Theta\left\{\left[\cos\Theta + \frac{r}{R}\sin^2\Theta\left(1 - \left(\frac{r}{R}\right)^2 \sin^2\Theta\right)^{-1/2}\right]\left[-\frac{r}{R}\cos\Theta + \left(1 - \left(\frac{r}{R}\right)^2 \sin^2\Theta\right)^{1/2}\right]^{-n}\right\}$$

ϵ_{gs} and σ_{gs} are the energy and size parameter between the LJ particle and the solid wall. ρ_s is the number density of interaction sites in the solid wall. The pore wall was set as a silica-like solid. Interactions with silicon atoms were neglected, and only the oxygen atoms were considered as the interaction sites as in many of the previous works for this kind of material.[11] The parameters ϵ_{gs}/k and σ_{gs} were 147.8 K and 0.32 nm, respectively.[12,13] Other constants were: the mass of the nitrogen $m = 4.653 \times 10^{-26}$ kg, the reduced temperature $T^* = Tk/\epsilon = 0.814$, and the number density of oxygen in silica $= 5.982 \times 10^{28}$ m^{-3}. The above parameters were determined so as to represent a real nitrogen-silicate standard isotherm faithfully.[12,13] Note that, however, our intention was not to mimic an adsorption isotherm, but to obtain adsorption isotherms on which the model would be tested. Thus the whole above setting is an example, and it would not in any sense bring a limitation to the applicability of the model: e.g., one may bring any potential function into the model that may be suitable to express the interaction between an adsorbate and a pore wall for a given adsorption system.

A simulation run for a given number of adsorbate particles started from an initial configuration arranged as a face-centered cubic lattice within the cylindrical wall. The initial velocity of each particle was given so as to attain the Maxwell−Boltzmann distribution at the given temperature. The temperature of the system was controlled by velocity scaling in the usual manner once for every 100 steps. The Verlet method was used to integrate the equations of motion numerically. Each run consisted of at least 5×10^5 up to 1×10^8 integration steps with a time increment of 1.0×10^{-14} s, the duration of which was decided so that the number of particles reaching the border plane counted about 500 or more. With the frequency f_B, or the number of reaching particles per unit time and per unit area at the border, the vapor-phase pressure p_g can be calculated with eq 13 assuming ideal behavior in the imaginary gas phase.[2]

$$p_g = f_B\sqrt{2\pi mkT} \quad (13)$$

The saturated vapor pressure for the model LJ fluid was determined by a simulation of the liquid state as described below, with which the equilibrium pressure was normalized to give relative pressure.

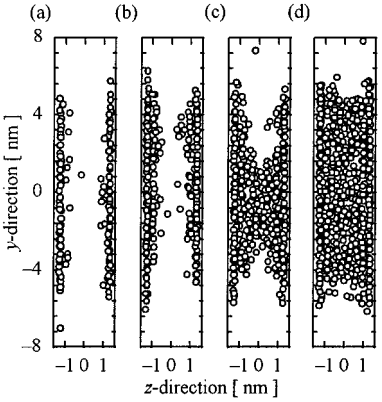

Figure 3. Sectional snapshots in a pore cross section between $x = 0.5$ nm and $x = -0.5$ nm obtained by MD simulation for a cylindrical pore with a diameter of 3.2 nm. (a) $N = 500$, $p_g/p_{sat} = 0.092$, (b) $N = 700$, $p_g/p_{sat} = 0.17$, (c) $N = 900$, $p_g/p_{sat} = 0.17$, (d) $N = 1200$, $p_g/p_{sat} = 0.37$.

3.3. Physical Properties of the Model Fluid. For testing the present model, some physical properties of the model adsorbate employed in this ideal experiment must be known: the saturated vapor pressure, the volume per molecule and the gas−liquid surface tension—all for bulk liquid. Thus, we simulated a liquid film consisting of the adsorbate particle in the rectangular cell by the MD method. We took a system of 2500 particles in a box of dimensions $L_x \times L_y \times L_z = 16.8\sigma_{gg} \times 16.8\sigma_{gg} \times 43.2\sigma_{gg}$ following the literature.[14−17] Similar to the simulations in a pore, a border plane with an imaginary gas phase was placed at each end of the cell in the vertical direction with sufficient distance from the liquid film. The run consisted of 1.2×10^6 integration steps of $\Delta t = 1 \times 10^{-14}$ s. Saturated pressure was also determined by the particle counting method.[2,7] The surface tension was calculated with the following statistical mechanical expression:

$$\gamma = \frac{1}{L_x L_y}\left\langle\sum_{ij}\frac{r_{ij}^2 - 3z_{ij}^2}{r_{ij}}\frac{d\phi(r_{ij})}{dr_{ij}}\right\rangle \quad (14)$$

The reduced values $p_{sat}\sigma_{gg}^3/\epsilon_{gg}$, V_p/σ_{gg}^3, and $\gamma\sigma^2_{gg}/\epsilon_{gg}$ were determined by the running average from 2×10^5 to 1.2×10^6 steps to be 0.0085, 1.29, and 0.627, respectively.

4. Results and Discussion

4.1. Adsorption Isotherm. Several runs for each pore size were conducted with various numbers of particles ranging from 500−1200 to obtain the adsorption equilibrium relation. Figure 3 shows cross sectional snapshots of molecules in a slice of pore space between $x = 0.5$ nm and $x = -0.5$ nm for a cylindrical pore with a diameter of 3.2 nm: (a) $N = 500$, $p_g/p_{sat} = 0.092$; (b) $N = 700$, $p_g/p_{sat} = 0.17$; (c) $N = 900$, $p_g/p_{sat} = 0.17$; (d) $N = 1200$, $p_g/p_{sat} = 0.37$. The surface adsorption phase is seen under low relative pressures, and the condensation phase develops under high relative pressures. The important point to be noted here would be that the surface adsorption state (b) and the condensed state (c) show almost the same

(11) Heuchel, M.; Snurr, R. Q.; Buss, E. *Langmuir* **1997**, *13*, 6795.
(12) Macelroy, J. M. D.; Raghavan, K. *J. Chem. Phys.* **1990**, *93*, 2068.
(13) Brodka, A. *Mol. Phys.* **1994**, *83*, 803.
(14) Chapela, G. A.; Saville, G. *J. Chem. Soc., Faraday Trans. 2* **1977**, *73*, 1133.
(15) Nijmeijer, M. J. P.; Bakker, A. F.; Bruin, C. *J. Chem. Phys.* **1988**, *89*, 3789.
(16) Holcomb, C. D.; Clancy, P.; Zollweg, J. A. *Mol. Phys.* **1993**, *78*, 437.
(17) Chen, L. *J. Chem. Phys.* **1995**, *103*, 10214.

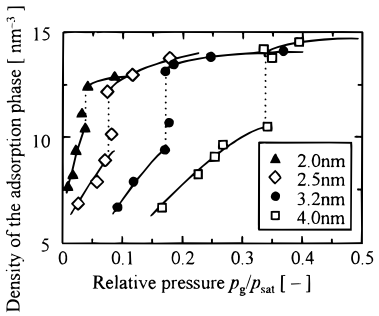

Figure 4. Adsorption isotherms obtained with MD simulations. The capillary coexistence conditions are indicated by the vertical dotted lines.

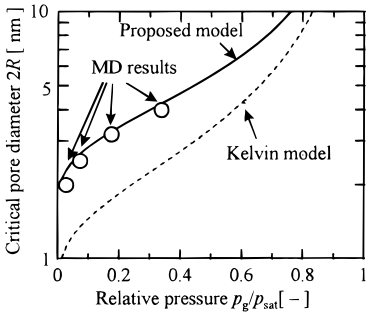

Figure 5. Capillary coexistence curves: solid line, calculated by proposed model; dashed line, the Kelvin model; open circles, MD simulation results.

equilibrium vapor pressure despite the complete difference in the adsorbed state. This equality means that the isotherm is almost vertical at this vapor pressure, and does not show hysteresis.

The averaged densities of the fluid in pores at the central portion of the cell, where the density is not affected by the interface, were evaluated from the data after 2000 ps, and plotted against the relative pressures in Figure 4. An almost vertical change in the density can be recognized for each pore size. The critical condensation pressures were determined from the rise of the isotherms.

4.2. Critical Condensation Pressure. The performance of the present model in predicting the critical condensation pressure for a given pore size is tested here with the above results of MD simulations.

The potential function $\Delta\psi$ in the model is obtained by subtraction of the potential energy of the adsorbate liquid state from the potential of the pore wall. Further, only the attractive term of the potential would be large enough to be considered. The repulsive term can be neglected because the effect of repulsive potential decreases rapidly with the distance from a pore wall, and it hardly influences the condensation phenomena in the inner portion of the pore. According to the setting in the MD simulations, the attractive potential from the pore wall ϕ_{gs} is

$$\phi_{gs} = -\pi\epsilon_{gs}\rho_s\sigma_{gs}{}^6K_3(r, R) \quad (15)$$

The potential that a molecule would feel if the pore wall consisted of liquid of adsorbate ϕ_{gg} is expressed as follows, considering the cutoff distance for adsorbate−adsorbate interaction.

$$\phi_{gg} = -\pi\epsilon_{gg}\rho_g\sigma_{gg}{}^6K_3(r, R) - (-\pi\epsilon_{gg}\rho_g\sigma_{gg}{}^6K_3(r, r + 3.5\sigma_{gg})) \quad (16)$$

where ρ_g is the number density of adsorbate particles in liquid state. Here, if $r + 3.5\sigma_{gg} < R$, eq 16 becomes $\phi_{gg} = 0$.

Thus the function will be:

$$\Delta\psi = \phi_{gs} - \phi_{gg} = -\pi(\epsilon_{gs}\rho_s\sigma_{gs}{}^6 - \epsilon_{gg}\rho_g\sigma_{gg}{}^6)K_3(r, R) - \pi\epsilon_{gg}\rho_g\sigma_{gg}{}^6K_3(r, r + 3.5\sigma_{gg}) \quad (17)$$

The rightmost term with the cutoff distance is used only for the accord with the model fluid employed in the simulation. When applying the model to a real experimental system, one need not include the term.

Using eq 17 and the physical properties described in Section 3.3., the critical condensation pressure for each pore size is calculated by the present model and compared with the simulation results in Figure 5 and Table 1, together with the Kelvin model for which the "physical properties" of the LJ particle were commonly used. Again, significant underestimation in pore size by the Kelvin model (dashed line) is recognized. On the other hand the proposed model (solid line) predicts almost perfectly the results of the MD simulations (open circles), to show its reliability.

Table 1. Comparison of Capillary Coexistence Conditions

relative pressure	0.02−0.03	0.07	0.17−0.19	0.34
MD simulation (nm)	2.0	2.5	3.2	4.0
proposed model (nm)	2.2−2.3	2.6	3.2−3.3	4.2
Kelvin model (nm)	1.1	1.3	1.7−1.8	2.4

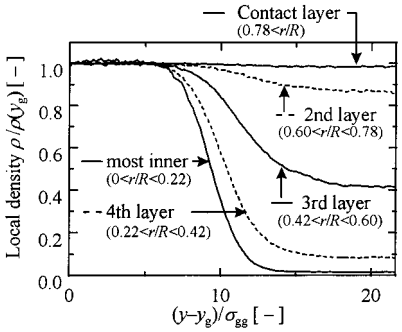

Figure 6. Density profile in longitudinal direction at various r under the critical condensation pressure for D = 4.0 nm.

4.3. Shape of the Gas−Condensate Interface. Figure 6 shows local density profiles in a pore of 4 nm, under critical conditions, along the y-direction. The radial intervals shown in the figure stand for each adsorption/condensation layer over which the densities were averaged. As for the pseudo-layer structure, further discussion is made in the next section. y_g denotes the position of the center of gravity, and the densities are normalized with that at y_g for each radial section. The averaging calculation was done over 1.0×10^6 MD steps.

Near the central portion of the pore, the density varies over a thickness of ca. $5\sigma_{gg}$ from that at the condensed part down to almost zero at the noncondensed part of the cell. As we approach the wall, the density variation becomes broader, and the lower plateau gains a finite density because of the existence and influence of the surface adsorption phase. For the section closest to the wall, the density shows only a flat profile because it corresponds to a position within the surface adsorption phase. We determined the position of the interface from the equimolar dividing surface for each density profile, to yield the shape of the interface.

Figure 7 compares the results of the MD simulation and the model prediction by eq 9 shown by a solid line, together with the dashed line which indicates the hemi-

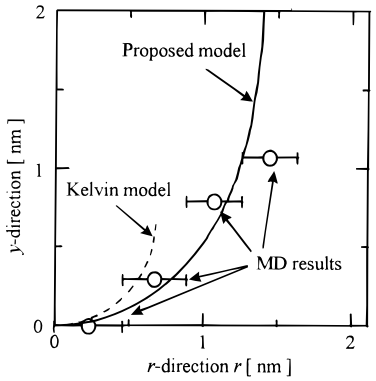

Figure 7. Comparison of the shape of the gas−condensate interface under critical condensation conditions: solid line, calculated by proposed model; dashed line, the Kelvin model; open circles, MD simulation results determined from the density distribution in Figure 6.

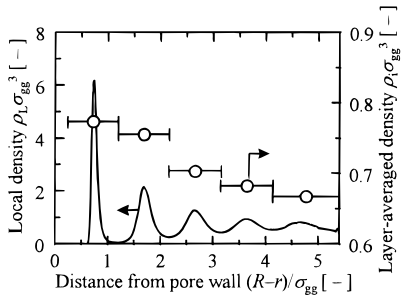

Figure 8. Local density profiles over radial direction within a pore of 4 nm under the critical condensation pressure. Averaged density for each layer is also plotted by the open circle with the bar indicating the range of averaging.

spherical interface given by the Kelvin model under the same relative pressure. It clearly demonstrates that the curvature in the proposed model is weaker than that expected by the Kelvin model, which reflects the contribution of the pore-wall potential energy on forming the condensed phase in the proposed model. The positions of interface observed in the MD simulation (open circles with bars indicating averaging sections) show a somewhat skewed shape that differs from a circular arc in a similar way to our model. Though the detailed quantitative agreement might not be sufficient, the shape of interface in the simulation is thought to be in quite good accord with the proposed model.

4.4. Pressure Profile. The proposed model is based on the continuum assumption and isotropic pressure, while in the molecular simulation the discrete nature of LJ particles and the tensor feature of the pressure in the condensed phase would prevail. As a compromise for testing our model from the viewpoint of the pressure, a layer-averaged density and corresponding bulk pressure were considered as follows.

The density profile with respect to the r-direction $\rho_L^*(r)$ was calculated within the central portion of the cell between $y = y_g + 0.5\sigma_{gg}$ and $y = y_g - 0.5\sigma_{gg}$. An example for pore of 4 nm under critical condensation conditions is shown in Figure 8. A layering structure is observed over the pores as expected. Next, a layer-averaged density for individual layer ρ_i was calculated with boundaries on the average being the positions at which the local densities $\rho_L(r)$ exhibit minima. The average density of the individual adsorbed layer is plotted also in Figure 8, which shows a gradual decrease toward the center of the pore.

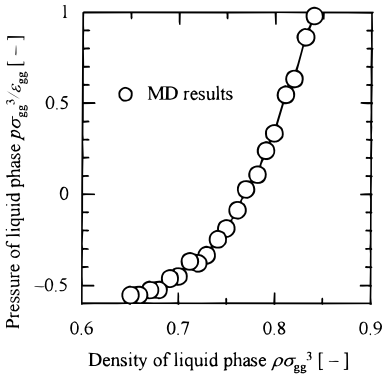

Figure 9. Density−pressure relation for liquid phase calculated by the virial theorem from MD simulation results in the homogeneous phase.

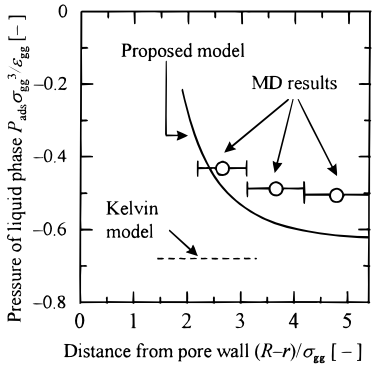

Figure 10. Comparison of pressure profile over the radial direction within the condensed phase under critical condensation conditions: solid line, calculated by proposed model; dashed line, the Kelvin model; open circles, pressure corresponding to the local density within the pore observed in the MD simulation.

Separately, we obtained the relation between the pressure and the density for bulk liquid by using MD simulations of LJ particles in a cube with each length of $7\sigma_{gg}$. The run consisted of 2000 integration steps of 1×10^{-14} s. The pressure of the homogeneous liquid phase was calculated according to the usual manner employing the virial theorem.

$$p = \frac{N}{V}kT - \frac{1}{3V}\left\langle \sum_{i<j} r_{ij} \frac{d\phi(r_{ij})}{dr_{ij}} \right\rangle \qquad (18)$$

The reduced pressure $p\sigma_{gg}^3/\epsilon_{gg}$ was determined against liquid densities as in Figure 9.

From the averaged density of an individual layer a corresponding bulk pressure for the MD simulation results was determined as shown in Figure 10 (open circles), where the estimates by the proposed model (solid line) and the Kelvin model (dashed line: constant) are also illustrated. The MD simulation results show that the condensation phase has a negative pressure near the pore center and the pressure becomes higher toward the pore wall, which could never be explained by the conventional model with uniform pressure within the condensed phase. The prediction of the proposed model is in quite good accord in this aspect. Also quantitatively, the agreement is thought to be satisfactory considering uncertainties and difficulties involved, e.g., in the above averaging process and in pressure determination. The fair agreement in pressure distribution in the condensate would be thought to add another proof for the reliability of this nonuniform model for the pore size determination.

5. Conclusion

We proposed a new condensation model for cylindrical pores that takes account of the effect of the attractive potential energy from pore walls and the surface tension deviated from that of a flat interface. For verification of the condensation model, MD simulations were conducted to determine the critical condensation pressures for various sizes of pores. The model, with its simple concept and handy calculation, successfully described the capillary coexistence relation given by the MD simulations. The model was tested also from the viewpoints of the shape of the interface and the pressure distribution within the condensed phase. Since the model treats fluid in a pore as a continuum throughout, a lower limit in pore size must exist where this assumption should break down. However, the model was effective in a pore as small as 2 nm in diameter. This limitation was thought to be smaller than 2 nm.

Appendix A: Note on Applying the Gibbs−Tolman−Koenig−Buffs Equation in the Present Model

The surface tension depends on the curvature of the gas−liquid surface if the radius of interface approaches the interface thickness.[8] Thus, this effect should be taken into account to describe the condensation phenomena in nanopores. The relation between the radius and the tension is known as the Gibbs−Tolman−Koenig−Buff equation.[9] The equations for a spherical surface and a cylindrical one, respectively, can be expressed as

$$\frac{\gamma(\rho_i)}{\gamma_N} = 1 - 2\frac{\delta}{\rho_i} \tag{A1}$$

$$\frac{\gamma(\rho_i)}{\gamma_N} = 1 - \frac{\delta}{\rho_i} \tag{A2}$$

where $\gamma(\rho_i)$ is surface tension for a curved surface of radius ρ_i, and γ_N indicates that for a plane surface. δ is the distance between the equimolar dividing surface and the surface of tension within the interfacial region, which is positive for a liquid drop and negative for a bubble. The magnitude of δ was reported to be on the order of the molecular size or liquid-phase intermolecular distance, i.e., 0.3 ± 0.1 nm for simple molecules such as argon and nitrogen,[9] and this representative value was employed in the calculation.

In the present model the shape of the gas−condensate interface changes from spherical at $r = 0$ to cylindrical at $r = r_0$, which means that we should use eq A1 at the center and eq A2 near the wall. To establish a continuous variation between the two equations, we assumed the equation for an intermediate curved surface as

$$\frac{\gamma(\rho)}{\gamma_N} = 1 - \frac{\delta}{\rho} \tag{A3}$$

where $1/\rho$ is the sum of the two principal curvatures ($1/\rho_1 + 1/\rho_2$) as given in eq 2. The above expression reduces to eq A1 at the center of pores where $\rho_1 = \rho_2$, while at the surface of the adsorption film it becomes eq A2 where $1/\rho_1 = 0$.

Appendix B: The Necessity of the Surface Tension Term for the Adsorbed Film

We examined the contribution of the surface tension term in eq 7 by GCMC simulations, which compared adsorption on (1) a cylindrical surface and (2) a planar surface with the same potential energy. In a real adsorption system this kind of comparison could never be made because the overlap of potential energy in a cylindrical pore would naturally bring a stronger potential profile than that for a planar surface with same material. The simulation was made for adsorption on a planar solid surface with a fictitious potential that had the same $\Delta\psi$ as that for a cylindrical system with respect to the distance from the pore wall, and was compared with that within the normal cylindrical system under the same relative pressure. In other words, eq 7 was tested with common settings both in $\Delta\psi$ and p/p_{sat}, for the two kinds of geometry, to find out if a contribution of the curved surface of the adsorption phase would exist.

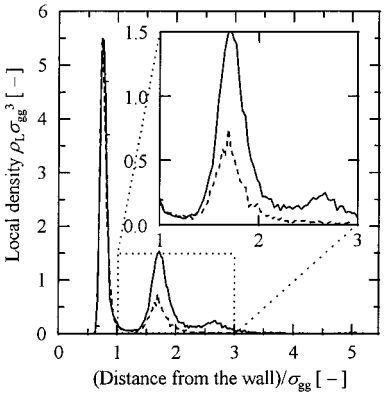

Figure 11. Local density distributions of surface adsorption film under $p\sigma_{gg}^3/\epsilon_{gg} = 0.0018$. Solid line: MC simulation result in the cylindrical pore. Dashed line: MC simulation result of the imaginary system.

In the cylindrical pore system (normal system), we used the periodic boundary condition for the longitudinal direction, and set a lower pressure than the critical condensation pressure. The length of the cell in the longitudinal direction and the pore diameter were $10.1\sigma_{gg}$ and $10.8\sigma_{gg}$ (4 nm), respectively. In the unit cell with the flat surface (imaginary system), we employed the usual manner of the periodic boundary condition for the transverse directions with the unit cell size of $10.1\sigma_{gg} \times 11.7\sigma_{gg}$. The cell height was $10.8\sigma_{gg}$ (2 nm), which was the same as the pore radius of the cylinder in comparison. The equilibrium pressure $p\sigma^3_{gg}/\epsilon_{gg}$ was set to be 0.0018 and each run consisted of at least 5×10^4 GCMC steps, each of which included N (number of particles) movement trials and N insertion or deletion trials.

Figure 11 shows the local density distributions in the two adsorption systems: The solid line is for the normal cylindrical system, and the dotted line is for the imaginary planar system. The curved adsorption phase gives greater density especially in the second and third layers. We calculated a statistical thickness of adsorption phase t that corresponds to the amount adsorbed in each system, using bulk liquid density usually employed for this purpose. The results were $t = 1.6\sigma_{gg}$ for the cylindrically curved adsorption phase, and $t = 1.1\sigma_{gg}$ for the flat case, which implies the existence of an enhancing effect in the former system as we expected. These values were compared further quantitatively with the predictions by eq 7. Using the physical properties of the LJ fluid the thickness of the adsorption film in the pore with diameter 4.0 nm was calculated to be $1.5\sigma_{gg}$, which is in reasonably good agreement with the simulation result, to support the appropriateness of eq 7 employed in the proposed model.

LA991227E